RSC Advances

PAPER

The effect of γ-Al$_2$O$_3$ surface hydroxylation on the stability and nucleation of Ni in Ni/γ-Al$_2$O$_3$ catalyst: a theoretical study†

Zhixue Liu,[a] Yuhan Wang,[b] Jingrui Li[a] and Riguang Zhang*[a]

Using recent well-defined models of γ-Al$_2$O$_3$ surfaces, the interactions of Ni$_n$($n = 1$–7) clusters with different γ-Al$_2$O$_3$ surfaces have been investigated in order to illustrate, by density functional theory periodic calculations, the effect of γ-Al$_2$O$_3$ surface hydroxylation on the stability and nucleation of Ni in Ni/γ-Al$_2$O$_3$ catalyst. Three types of γ-Al$_2$O$_3$ surfaces, dehydrated γ-Al$_2$O$_3$(100), dehydrated γ-Al$_2$O$_3$(110) and hydrated γ-Al$_2$O$_3$(110) were considered. Our results show that for the adsorption of Ni$_n$($n = 3$–7) clusters, the γ-Al$_2$O$_3$(110) surface is more favorable than the γ-Al$_2$O$_3$(100) surface, however, for single Ni atoms and Ni$_2$ clusters, the reverse becomes true. Meanwhile, for the adsorption of Ni$_n$($n = 2$–7) clusters, the hydrated (110) surface is not favorable compared to the dehydrated (110) surface, due to the presence of surface hydroxyls on the former. The reverse is true for single Ni atoms due to weaker surface deformation. Further, the support stabilizes Ni$_n$($n = 2$–7) clusters well in the supported state, in which the presence of surface hydroxyls reduces the stability of the supported Ni$_n$ clusters. On the other hand, the nucleation ability of Ni$_n$ clusters on different γ-Al$_2$O$_3$ surfaces, is more favorable on the γ-Al$_2$O$_3$(110) surface than on the γ-Al$_2$O$_3$(100) surface, and the dehydrated (110) surface is more favorable than the hydrated (110) surface due to the presence of surface hydroxyls, namely, surface hydroxylation reduces the nucleation ability of Ni$_n$ clusters on the γ-Al$_2$O$_3$ surface. More importantly, the exothermicity of supported Ni$_n$($n = 2$–7) clusters on different γ-Al$_2$O$_3$ surfaces is lower than that of isolated Ni$_n$ clusters, indicating that the support is not favorable for the nucleation of Ni$_n$($n = 2$–7) clusters, as a result, the support can inhibit the aggregation of clusters, and favors the formation of small clusters.

1. Introduction

Oxide-supported metal catalysts play a pivotal role in a lot of technologically important applications, including sensors, solid oxide fuel cells, and heterogeneous catalysts.[1] Among the oxide-supported metal catalysts, Ni-based catalysts are often used in industrial processes such as the hydrogenation, hydrotreatment and hydrogenolysis of hydrocarbons, steam reforming of hydrocarbons, and methanation.[2–5] Different supports are widely used to disperse Ni particles, such as γ-Al$_2$O$_3$,[6,7] TiO$_2$,[8] CeO$_2$,[9] SiO$_2$ [10,11] or La$_2$O$_3$,[7] among them, γ-Al$_2$O$_3$ is one of the most common supports as its large surface area and high degree of porosity favors the good dispersion of active species.[12]

Hydroxylation is a common process that occurs in many processes.[13–18] For the oxide-supported metal catalysts, the hydroxylation of the oxide support has an effect on the metal–support interaction, and further on the reactions taking place on the catalyst.[19–24] For example, Cu(111) and Cu/TiO$_2$(110) are both active towards the water–gas shift (WGS) reaction, however, due to the surface hydroxylation of the TiO$_2$ support, the Cu/TiO$_2$(110) catalyst has a much higher catalytic activity in the WGS reaction than the Cu(111) catalyst.[19] For γ-Al$_2$O$_3$-supported metal catalysts, under normal reaction conditions, the surface of the γ-Al$_2$O$_3$ support inevitably becomes hydrated/hydroxylated; subsequently, the surface nature of the support changes,[22–29] this change affects both the metal–support interaction and the reactions taking place over the catalyst. For example, Valero *et al.*[30] have investigated the effect of γ-Al$_2$O$_3$ surface hydroxylation on the stability and diffusion of a single Pd atom, and found that the binding energy of the Pd atom decreases as the OH coverage of the γ-Al$_2$O$_3$ surface increases. In addition, previous studies have shown the effect of γ-Al$_2$O$_3$ surface hydroxylation on the selectivity of CO$_2$ hydrogenation over different Ni/γ-Al$_2$O$_3$,[27] Pd/γ-Al$_2$O$_3$ [31] and Cu/γ-Al$_2$O$_3$ [32] catalysts, suggesting that the hydroxylation of the γ-Al$_2$O$_3$ surface can alter the reaction pathway and the selectivity of CO$_2$ hydrogenation.

[a]Key Laboratory of Coal Science and Technology of Ministry of Education and Shanxi Province, Taiyuan University of Technology, No. 79 Yingze West Street, Taiyuan 030024, Shanxi, China. E-mail: zhangriguang@tyut.edu.cn; zhangriguang1981@163.com; Fax: +86 351 6041237; Tel: +86 351 6018239

[b]School of Chemical Engineering and Environment, Beijing Institute of Technology, Beijing 100081, China

† Electronic supplementary information (ESI) available: details of the adsorption of Ni$_n$ clusters on dehydrated and hydrated γ-Al$_2$O$_3$(110) surfaces, as well as the corresponding most stable configurations of Ni$_n$ clusters. See DOI: 10.1039/c3ra46352d

On the other hand, the activity and selectivity of metal-supported catalysts are strongly influenced by the size of the dispersed metal particles, and the metal–support interaction.[33–38] Small metal clusters or particles have interesting properties for catalytic processes due to the presence of low-coordination atoms and electron confinement effects,[39] which is different from those of bulk metals. For example, Zhang et al.[31] have suggested that the presence and number of low-coordinated Pd particles on a Pd/γ-Al$_2$O$_3$ catalyst is of great importance to improve the overall activity and selectivity of CO$_2$ hydrogenation. The *quasi in situ* X-ray photoelectron studies of Loviat et al.[6] have shown that the reactivity and the observed reaction mechanisms for methane production from syngas using a Ni/γ-Al$_2$O$_3$ catalyst are directly influenced by both the size and the composition of the Ni particle on the γ-Al$_2$O$_3$ support. Moreover, on the basis of EXAFS and IR spectra studies using an Ir/γ-Al$_2$O$_3$ catalyst, Argo et al.[35] have pointed out that the rate of ethene hydrogenation on Ir$_4$ clusters is typically several times greater than that on Ir$_6$ clusters. Further, Prasad and co-authors[37,38] and Meier et al.[40] also pointed out that the metal cluster size, the support material, or both, are critical in determining the catalytic activity.

Nowadays, Ni/γ-Al$_2$O$_3$ catalyst is widely used in many chemical processes such as hydrogenation,[27] dehydrogenation, reformation,[41] methanation, desulfurization, methane oxidation, and in the production of many bulk and fine chemicals.[42–47] Unfortunately, it is often difficult to obtain pertinent information from experiments on the metal–support interaction in Ni/γ-Al$_2$O$_3$ catalyst, as well as the stability and nucleation of metals on supports with different properties. Theoretical calculations are a valuable tool to complement experimental results, and a detailed investigation of metal–support interactions, as well as the study of the stability and nucleation of metals on the support at the molecular level not only help to increase the understanding of the underlying interaction mechanisms, but also serve as the basis for the selective design of Ni-based catalysts to improve the catalytic performance towards the desired reaction. A number of theoretical studies have examined the stability and nucleation of metals on an Al$_2$O$_3$ support, including Pd on γ-Al$_2$O$_3$,[48] Rh on γ-Al$_2$O$_3$,[49] Cu on α-Al$_2$O$_3$[50] and γ-Al$_2$O$_3$,[51] as well as Ag on α-Al$_2$O$_3$(0001).[52] For example, Valero et al.[48] have shown that with a very low metal coverage, the surface hydroxylation of hydrated γ-Al$_2$O$_3$(110) surfaces is favorable for the nucleation of Pd, whereas, with a higher metal coverage, the reverse is true for dehydrated γ-Al$_2$O$_3$(100). Further, Shi et al.[49] have shown that the nucleation of Rh is better on hydrated γ-Al$_2$O$_3$ surfaces than on dehydrated surfaces. Hu et al.[53] have found that Pd$_{13}$ and Pt$_{13}$ clusters are more stable on a dehydrated γ-Al$_2$O$_3$(100) surface than on a hydrated γ-Al$_2$O$_3$(110) surface. However, to our knowledge, little attention has been paid to the effect of γ-Al$_2$O$_3$ surface hydroxylation on the stability and nucleation of Ni in a Ni/γ-Al$_2$O$_3$ catalyst.

In this study, by using density functional theory (DFT) method, we present a detailed and systematic theoretical investigation of the stability and nucleation of small Ni$_n$(n = 1–7) clusters on three different γ-Al$_2$O$_3$ surfaces including the dehydrated (100), dehydrated and hydrated (110) surfaces. The objective was twofold: (i) to identify the preferred adsorption site, and how the isolated Ni$_n$ clusters were modified after adsorption on the three different γ-Al$_2$O$_3$ surfaces, and (ii) to explore the effect of γ-Al$_2$O$_3$ surface hydroxylation on the stability and nucleation of Ni in Ni/γ-Al$_2$O$_3$ catalyst.

2. Models and methods

2.1 Computational models

Both spinel and non-spinel structure models have been proposed for γ-Al$_2$O$_3$.[54–63] The non-spinel model has been well characterized both experimentally and computationally.[54–63] Moreover, the non-spinel model can produce diffraction patterns that are close to the characteristic diffraction patterns of γ-Al$_2$O$_3$.[58–60] Further, the non-spinel γ-Al$_2$O$_3$ model has been widely used to construct surfaces in previous studies,[62,64,65] thus, we employed the non-spinel-γ-Al$_2$O$_3$ as presented in previous studies to model the γ-Al$_2$O$_3$ surface in this study. The corresponding bulk model of the non-spinel-γ-Al$_2$O$_3$ used was taken from a previous theoretical investigation[62] of the calcination of boehmite, the hydrated precursor of γ-Al$_2$O$_3$, in which a wide range of aluminum atom distributions in this oxygen atom matrix was simulated, and the most stable structure with 25% of tetrahedral aluminum was retained as the best model for γ-Al$_2$O$_3$, as shown in ref. 55.

On the other hand, it has been reported in ref. 55 and 63 that by using the neutron diffraction analysis method of Beaufils and Barbaux,[66] the (110) surface was estimated to be 83% of the total surface area, whereas the (100) surface was 17% of the total surface area. In addition, the electron microscopy study carried out by Nortier et al.,[67] confirmed that the (110) surface is the predominant facet, covering about 70% of the total surface area, the remaining 30% corresponding to the (100) and (111) surfaces. Further, the (100) surface was found to be poorly hydrated under a broad range of experimental conditions.[68] Thus, in this study, we chose the (110) and (100) surfaces to study the stability and nucleation of Ni using DFT slab calculations. The (100) surface was modeled by a (2 × 1) supercell with a dimension of 11.17 × 8.41 × 20.44 Å, and included ten atomic layers, as shown in Fig. 1(a). The vacuum region was set to 12 Å in order to separate the slabs in the direction perpendicular to the surface. During geometry optimization, the bottom four layers were frozen in their bulk position, whereas, the remaining six layers together with the adsorbed Ni$_n$(n = 1–7) clusters were allowed to relax. For the γ-Al$_2$O$_3$(110) surface, the dehydrated and hydrated surfaces were considered. The supercell for the (110) surface included six layers with a vacuum region of 12 Å, resulting in a supercell size of 8.41 × 8.07 × 19.17 Å. In this case, the adsorbed Ni$_n$(n = 1–7) clusters and/or hydroxyls together with the Al and O atoms in the top four layers were allowed to relax.

In the dehydrated γ-Al$_2$O$_3$(100) surface presented in Fig. 1(a), 5-fold-coordinated aluminum Al(1), Al(2) and Al(3), and 3-fold-coordinated oxygen O(A), O(B), O(C) and O(D) are exposed. For the dehydrated γ-Al$_2$O$_3$(110) surface, as shown in Fig. 1(b), the 3-fold-coordinated aluminum (Al$_{3c}$), 4-fold-coordinated aluminum (Al$_{4c}$), 6-fold-coordinated aluminum (Al$_{6c}$),
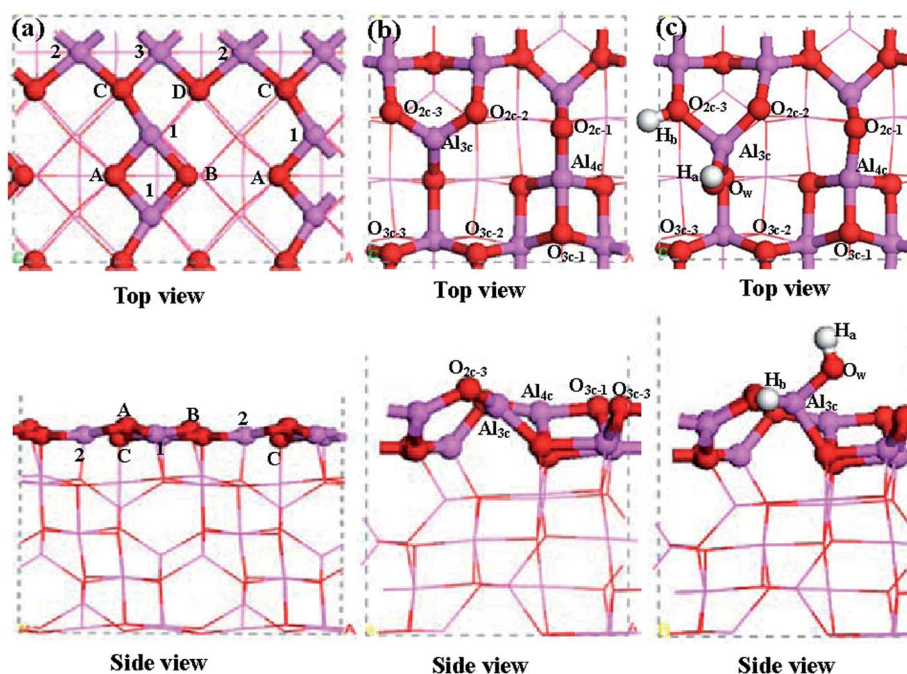
Fig. 1 The top and side views of (a) the dehydrated γ-Al₂O₃(100) surface, (b) the dehydrated γ-Al₂O₃(110) surface, and (c) the hydrated γ-Al₂O₃(110) surface. Pink, red and white balls stand for Al, O and H atoms, respectively.

2-fold-coordinated oxygen (O_{2c}), and 3-fold-coordinated oxygen (O_{3c}) atoms are exposed, of which Al_{3c}, Al_{4c}, O_2 are coordinately unsaturated.

For the hydrated γ-Al₂O₃(110) surface, under normal reaction conditions as demonstrated by Digne *et al.*,[55] the (110) surface inevitably becomes hydrated/hydroxylated, thus, a partially hydrated γ-Al₂O₃(110) surface was employed to characterize the effect of surface hydroxylation on the stability and nucleation of Ni in the Ni/γ-Al₂O₃ catalyst. The hydroxylated surfaces are formed by dissociative adsorption of water on the dry surface. The thermodynamics of hydroxylation with various OH coverages were studied by Digne *et al.*[55] However, our aim in this work was to study the qualitative effect of γ-Al₂O₃ surface hydroxylation on the stability and nucleation of Ni in the Ni/γ-Al₂O₃ catalyst, not to describe the specific hydroxyl coverage, which can vary under the given experimental conditions. As a result, only one H_2O molecule was considered for the hydrated γ-Al₂O₃(110) surface in this study. The previous DFT studies carried out by Pan *et al.*[29] investigated the hydroxylation process by the dissociation of one H_2O molecule on the dry γ-Al₂O₃(110) surface, which is the same as our model of the dry γ-Al₂O₃(110) surface, as shown in Fig. 1(b), their results showed that water dissociation across the O_{2c}–Al_{3c} bridge site is favorable both thermodynamically and kinetically, and the hydroxylation of the dry γ-Al₂O₃(110) surface is an activated process with only a very small barrier of 40.5 kJ mol^{-1}. Fig. 1(c) presents the side and top views of the partially hydroxylated γ-Al₂O₃(110) surface, in which one H_2O molecule dissociates into an hydroxyl (O_wH_a) with a bond length of 0.967 Å, which occupies the Al_{3c} site through an O_w–Al_{3c} bond (1.726 Å). Meanwhile, a proton (H_b) binds with a

neighboring O_{2c-3} site through the H_b–O_{2c-3} bond (1.027 Å). Thus, two hydroxyls are formed in each surface unit cell.

2.2 Computational methods

All the calculations were carried out in the framework of DFT using the Dmol³ program in the Materials Studio 4.4 package.[69,70] The generalized gradient approximation (GGA) corrected exchange-correlation functional proposed by the Perdew–Burke–Ernzerhof (PBE) functional[71] was employed with a double numerical basis set with polarization (DNP).[72] The inner electrons of Ni and Al atoms were kept frozen and replaced by an effective core potential (ECP),[73,74] and other atoms were treated with an all electron basis set. For optimization of the geometry, the forces imposed on each atom were converged to be less than 0.0004 Ha Å^{-1} (1 Ha = 2625.5 kJ mol^{-1}), the total energy was converged to be less than 2.0×10^{-5} Ha and the displacement convergence was less than 5×10^{-3} Å. A Fermi smearing of 0.005 Ha for orbital occupancy was used to improve the computational performance. In addition, the properties of isolated Ni_n clusters were calculated using a $15 \times 15 \times 15$ Å cubic unit cell, the charge transfer was calculated using Mulliken charge, and the dipolar correction was not considered in this study.

Different *k*-point grid samplings ranging from $(1 \times 1 \times 1)$ to $(4 \times 4 \times 1)$ were tested for both the bare (100) and (110) surface slabs, as well as the surfaces containing adsorbed Ni_4 clusters. The differences between the surface energies and Ni_4 cluster adsorption energies were found to be negligible using the $(2 \times 2 \times 1)$, $(3 \times 3 \times 1)$, and $(4 \times 4 \times 1)$ *k*-point grids for both surfaces. As a result, for a reasonable CPU cost, the $(2 \times 2 \times 1)$ *k*-point sampling scheme was employed in this work, and gave good converged results.

3. Results and discussion

In this section, we firstly investigate the stable configuration of isolated $Ni_n(n = 2–7)$ clusters in section 3.1, then, the adsorption of the most stable Ni_n clusters on three different γ-Al_2O_3 surfaces, and the stability of the Ni_n clusters are discussed in section 3.2, Further, the nucleation of Ni_n clusters on the three different γ-Al_2O_3 surfaces are studied in section 3.3. Finally, a comparison of the stability and nucleation between Ni and other metals is provided in section 3.4.

3.1 Structures of isolated $Ni_n(n = 2–7)$ clusters

Isolated Ni clusters have been widely studied previously.[6,75] In this section, details are given of the investigation of the geometries of isolated Ni_n clusters. To study the configuration of $Ni_n(n = 2–7)$ clusters, one-dimensional (1D), two-dimensional (2D), and three-dimensional (3D) structures were considered. And only the most stable geometries and key parameters of the $Ni_n(n = 2–7)$ clusters were considered, as listed in Table 1.

In order to evaluate the stability of isolated $Ni_n(n = 2–7)$ clusters, the average binding energy of isolated $Ni_n(n = 2–7)$ clusters, $E_{bind}(Ni_n)$, was calculated as follows:[51–53]

$$E_{bind}(Ni_n) = [E(Ni_n) - n \times E(Ni)]/n$$

where $E(Ni)$ is the total energy of the single Ni atom, n is the number of Ni atoms in the Ni_n clusters, herein, $n = 2–7$. With this definition, the smaller the $E_{bind}(Ni_n)$ the more stable the isolated $Ni_n(n = 2–7)$ cluster.

Table 1 The most stable geometry, the average Ni–Ni bond length, and the binding energy of the isolated $Ni_n(n = 2–7)$ clusters, $E_{bind}(Ni_n)$

n	Geometry	$\bar{d}(Ni–Ni)/Å$	$E_{bind}(Ni_n)/kJ\ mol^{-1}/atom$
2		2.163	−98.6
3		2.277	−144.5
4		2.354	−171.1
5		2.361	−198.9
6		2.413	−211.9
7		2.411	−227.7

For Ni_2 clusters, the Ni–Ni bond length and the average binding energy were 2.163 Å and −98.6 kJ mol⁻¹, respectively, which is in accordance with the experimental results.[76,77] For Ni_3 clusters, the most stable configuration is a 2D planar one, the average Ni–Ni bond length and the average binding energy were 2.277 Å and −144.5 kJ mol⁻¹, respectively. For Ni_4 clusters, the isolated 3D tetrahedral configuration is more stable than the isolated 2D planar one, which is in accordance with the corresponding Pd_4 clusters,[78] the average Ni–Ni bond length and the binding energy of Ni_4 clusters were 2.354 Å and −171.1 kJ mol⁻¹, respectively. For Ni_5 clusters, the most stable configuration is a trigonal bipyramid with an average Ni–Ni bond length of 2.361 Å, which is in agreement with the previous results of Reuse et al.,[75] the average binding energy of the Ni_5 clusters was −198.9 kJ mol⁻¹. For Ni_6 clusters, the average Ni–Ni bond length and the binding energy were 2.413 Å and −211.9 kJ mol⁻¹, respectively. Finally, the most stable configuration of Ni_7 clusters is a pentagonal bipyramid, which is similar to that of Pd_7[79] and Ag_7[52] clusters, the average bond length and the binding energy for Ni_7 clusters were 2.411 Å and −227.7 kJ mol⁻¹, respectively.

On the basis of the above results, we can see from Table 1 that the average Ni–Ni bond length in $Ni_n(n = 2–7)$ clusters was shorter than that in the bulk structure ($d(Ni–Ni) = 2.492$ Å), and the average Ni–Ni bond length increases with an increase of the cluster size, however, it cannot reach the corresponding bulk value. Meanwhile, with an increase of atomic coordination in the $Ni_n(n = 2–7)$ clusters, the value of the $E_{bind}(Ni_n)$ decreases.

3.2 Ni_n clusters adsorbed on different γ-Al_2O_3 surfaces

$Ni_n(n = 1–7)$ clusters were adsorbed on all possible positions of the γ-Al_2O_3 surfaces, here, only the most stable adsorption configurations are reported according to the adsorption energy, which is calculated as follows:[25,51]

$$E_{ads} = E(Ni_n/\gamma\text{-}Al_2O_3) - E(\gamma\text{-}Al_2O_3) - E(Ni_n)$$

where $E(\gamma\text{-}Al_2O_3)$ is the total energy of the bare γ-Al_2O_3 surface, $E(Ni_n)$ is the total energy of the isolated Ni_n clusters, and $E(Ni_n/\gamma\text{-}Al_2O_3)$ represents the total energy of Ni_n supported on the γ-Al_2O_3 surface. The adsorption energy can be broken down into the contributions of deformation energy and metal–support interaction energy to analyze the chemisorption process. During this process, the two partners (the γ-Al_2O_3 surface plus $Ni_n(n = 1–7)$ clusters) are deformed with respect to their isolated geometries.

Distortion of the surface or the metal cluster alone towards the geometry needed to overcome some energy is defined as the surface or metal cluster deformation energy. The surface deformation energy is calculated as follows:[25,51]

$$E_{def,surface} = E(\gamma\text{-}Al_2O_3{}') - E(\gamma\text{-}Al_2O_3)$$

where $E(\gamma\text{-}Al_2O_3{}')$ is the total energy of the surface with deformed geometry obtained after Ni_n cluster adsorption. With this definition, lower the $E_{def,surface}$ results in weaker surfaces.

The deformation energy of the $Ni_n(n = 1–7)$ clusters is calculated in a similar way:[25,51]

$$E_{\text{def},Ni_n} = E(Ni_n') - E(Ni_n)$$

where $E(Ni_n')$ is the total energy of the Ni_n clusters supported on the γ-Al_2O_3 surface. With this definition, the lower the E_{def,Ni_n} the weaker the cluster deformation is.

The interaction between the Ni_n clusters and the support is another key parameter. The metal–support interaction energy, E_{MSI}, is calculated as follows:[25,51]

$$E_{\text{MSI}} = E(Ni_n/\gamma\text{-}Al_2O_3) - E(Ni_n') - E(\gamma\text{-}Al_2O_3')$$

E_{MSI} is simply the adsorption energy between the already deformed partners, *i.e.*, without the energy contributions of geometry deformation in either fragment of the Ni/γ-Al_2O_3 system.

Therefore, the adsorption energy can be decomposed according to the following equation:[25,51]

$$E_{\text{ads}} = E_{\text{MSI}} + E_{\text{def},Ni_n} + E_{\text{def,surface}}$$

This energy decomposition scheme clearly shows that adsorption energy is a trade-off between two antagonistic effects: metal–support interaction energy and deformation energy.

3.2.1 Dehydrated γ-$Al_2O_3(100)$ surface. $Ni_n(n = 1–7)$ clusters were placed on the large number of well-defined adsorption sites that are available on the dehydrated γ-$Al_2O_3(100)$ surface, Fig. 2 presents the most stable adsorption configurations, Table 2 lists the corresponding key parameters of these configurations.

For single Ni atoms, it is preferrable to occupy the bridge site along O(C)–O(D) with an adsorption energy of -352.2 kJ mol^{-1}, as shown in Fig. 2(a), and $0.027e$ was transferred to support the surface from single Ni atoms. The adsorption of a single Ni atom can lead to strong surface deformation of the dehydrated γ-$Al_2O_3(100)$ surface with a surface deformation energy of 124.0 kJ mol^{-1}, this has also been observed in previous studies of the adsorption of single Rh atoms,[49] Pd atoms[48] and Cu atoms.[51] The bond lengths of Ni–O(C) and Ni–O(D) were 1.866 and 1.905 Å, respectively. The Ni$_1$–support interaction energy was -476.2 kJ mol^{-1}, which makes a major contribution to the adsorption energy.

For Ni$_2$ clusters, the most stable configuration is shown in Fig. 2(b), which is different from that of Cu$_2$ clusters.[51] In this configuration, two Ni atoms interact directly with the surface sites: the Ni$_1$ atom occupies the O(C)–O(D) bridge site with Ni$_1$–O(C), Ni$_1$–O(D) and Ni$_1$–Al(2) bond lengths of 1.895, 1.905 and 2.267 Å, respectively, while the Ni$_2$ atom is located at the O(A)–O(B) bridge site with Ni$_2$–O(A) and Ni$_2$–O(B) bond lengths of 1.925 and 1.858 Å, respectively. The adsorption of Ni$_2$ clusters introduces strong surface deformation (219.2 kJ mol^{-1}). The Ni$_1$–Ni$_2$ bond length of the adsorbed Ni$_2$ clusters was stretched to 2.603 Å from 2.163 Å in the isolated Ni$_2$ clusters with a cluster deformation energy of 50.9 kJ mol^{-1}. The adsorption energy and the Ni$_2$–support interaction energy were -480.3 and -750.4 kJ

mol^{-1}, respectively, which are lower than the corresponding energies for single Ni atoms (-352.2 and -476.2 kJ mol^{-1}). Meanwhile, $0.038e$ was transferred to the Ni$_2$ clusters from the support surface. Thus, the decrease of adsorption energy is mainly due to the decrease of the Ni$_2$–support interaction.

As shown in Fig. 2(c), the most stable adsorption configuration of Ni$_3$ clusters resembles that of the Cu$_3$ clusters obtained in our previous work.[51] In this configuration, the plane of the Ni$_3$ clusters lies aslant relative to the (100) surface forming Ni$_1$–Al(2) (2.373 Å), Ni$_1$–O(C) (1.993 Å), Ni$_1$–O(D) (1.995 Å), Ni$_2$–O(A) (1.915 Å), Ni$_2$–O(B) (1.868 Å) and Ni$_3$–Al(1) (2.414 Å) bonds. The adsorption energy of the Ni$_3$ clusters was -374.4 kJ mol^{-1}, which is higher than that of the Ni$_2$ clusters (-480.3 kJ mol^{-1}). $0.145e$ was transferred to the Ni$_3$ clusters from the support surface. Meanwhile, the Ni$_3$–support interaction energy obviously increased to -569.1 kJ mol^{-1} from -750.4 kJ mol^{-1} for the Ni$_2$ clusters, which is mainly due to the increase of the adsorption energy of the Ni$_3$ clusters. Compared to the Ni$_2$ clusters (50.9 and 219.2 kJ mol^{-1}), the adsorption of Ni$_3$ clusters is accompanied by relatively weak cluster and surface deformations with corresponding energies of 41.6 and 153.1 kJ mol^{-1}.

As shown in Fig. 2(d), Ni$_4$ clusters interact with the surface *via* three Ni atoms, the Ni$_4$–support interaction energy was -567.3 kJ mol^{-1}, which is close to that of the Ni$_3$ clusters (-569.1 kJ mol^{-1}). The lengths of Ni$_1$–Al(2), Ni$_1$–O(D), Ni$_2$–O(A), Ni$_2$–O(B), Ni$_3$–O(C) and Ni$_3$–Al(1) bonds were 2.449, 1.879, 2.029, 2.023, 1.916 and 2.463 Å, respectively. The adsorption energy of the Ni$_4$ clusters (-442.8 kJ mol^{-1}) was lower than that of the Ni$_3$ clusters (-374.4 kJ mol^{-1}), meanwhile, the adsorption of Ni$_4$ clusters can lead to weaker cluster and surface deformations (3.9 and 120.6 kJ mol^{-1}) relative to those for Ni$_3$ clusters (41.6 and 153.1 kJ mol^{-1}), which is the main reason for the decrease of adsorption energy, and leads to $0.102e$ being transferred to the Ni$_4$ clusters from the support surface.

For the Ni$_5$ clusters, as shown in Fig. 2(e), the most stable configuration is a trigonal bipyramid with one Ni–Ni bond cleavage, and Ni$_5$ clusters interact with the surface *via* four Ni atoms. The adsorption energy (-431.7 kJ mol^{-1}) was slightly higher than that for Ni$_4$ clusters (-442.8 kJ mol^{-1}), and $0.204e$ was transferred to the Ni$_5$ clusters from the support surface. The Ni$_5$–support interaction energy (-600.1 kJ mol^{-1}) was lower than that of the Ni$_4$ clusters (-567.3 kJ mol^{-1}), which makes a major contribution to the adsorption energy for Ni$_5$ clusters. The cluster and surface deformation energies were 40.2 and 128.2 kJ mol^{-1}, respectively, which are higher than those for Ni$_4$ clusters (3.9 and 120.6 kJ mol^{-1}). The stronger cluster deformation of Ni$_5$ clusters is mainly due to the increase of adsorption energy. In the adsorption configuration, the bond lengths of Ni$_1$–Al(2), Ni$_2$–O(D), Ni$_2$–Al(1), Ni$_3$–O(B), Ni$_3$–O(A), Ni$_4$–O(C) and Ni$_4$–Al(1) were 2.411, 1.939, 2.598, 2.001, 2.014, 1.930 and 2.611 Å, respectively.

As shown in Fig. 2(f), five Ni atoms in the most stable adsorption configuration of Ni$_6$ clusters prefer to interact with the surface, and form two Ni–Al(2) bonds (2.545 and 2.630 Å), one Ni$_1$–O(D) bond (1.900 Å), three Ni–Al(1) bonds (2.519, 2.607 and 2.614 Å), one Ni$_2$–O(B) bond (1.881 Å), one Ni$_3$–O(A) bond (1.971 Å) and one Ni5–O(C) bond (1.897 Å). The adsorption
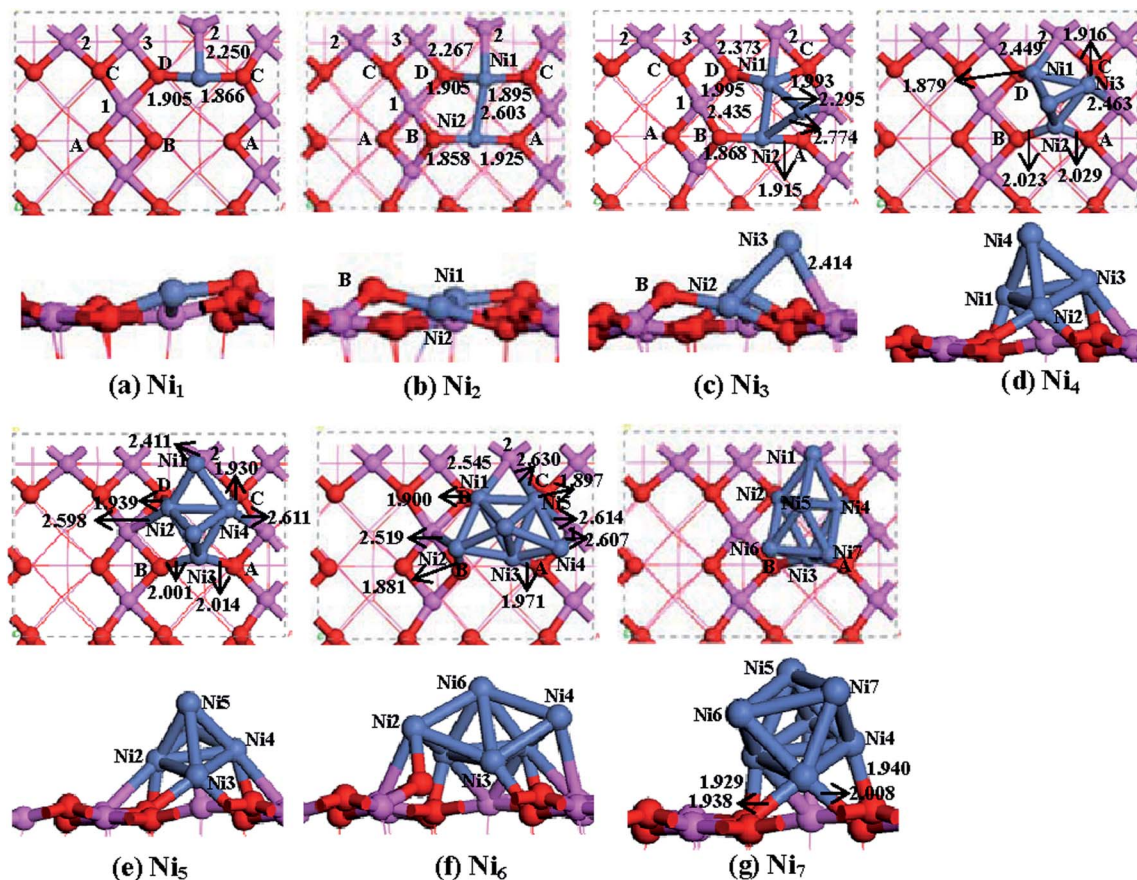
Fig. 2 The most stable adsorption configuration of $Ni_n(n = 1-7)$ clusters on the dehydrated γ-Al_2O_3(100) surface. Bond lengths are in Å. The blue balls represent Ni atoms, and the others are the same as in Fig. 1.

energy and the Ni_6–support interaction energy (-464.7 and -706.0 kJ mol^{-1}) were lower than those for the Ni_5 cluster (-431.7 and -600.1 kJ mol^{-1}), and $0.289e$ was transferred to the Ni_6 cluster from the support surface. The decrease of Ni_6–support interaction energy has a major effect on the adsorption energy. The adsorption of Ni_6 clusters on the surface leads to a stronger surface deformation (204.9 kJ mol^{-1}) than that of Ni_5 clusters (128.2 kJ mol^{-1}). The adsorption also leads to Ni_6 cluster deformation (36.4 kJ mol^{-1}), whereas, it is slightly weaker than that of the Ni_5 clusters (40.2 kJ mol^{-1}).

The most stable adsorption configuration of Ni_7 clusters is presented in Fig. 2(g), and is characterized by a strong adsorption (-493.5 kJ mol^{-1}) and a weak Ni_7–support interaction (-658.0 kJ mol^{-1}) in comparison with the adsorption of Ni_6 cluster (-464.7 and -706.0 kJ mol^{-1}). Upon adsorption to the dehydrated (100) surface, the pentagonal bipyramid structure of the Ni_7 clusters is distorted. The adsorption of Ni_7 clusters introduces both cluster and surface deformations with deformation energies of 42.6 and 121.9 kJ mol^{-1}, respectively, $0.232e$ was transferred from the support surface to the Ni_7 clusters. The decrease of the adsorption energy for the Ni_7 clusters was mainly due to the weaker surface deformation compared to that for the Ni_6 clusters (204.9 kJ mol^{-1}). In this stable configuration, four Ni atoms directly interact with the surface, and form two Ni–Al(2) bonds (2.468 and 2.655 Å), Ni_2–O(D) bond (1.929 Å),

Ni_3–O(B) bond (1.938 Å), Ni_3–O(A) bond (2.008 Å) and Ni_4–O(C) bond (1.940 Å).

From the obtained energy values listed in Table 2, we can obtain that on dehydrated (100) surface, for the adsorption of Ni_n cluster, Ni_n cluster deformation, surface deformation and Ni_n–support interaction, these four parameters have the strong correlation. The adsorption of Ni_n clusters on the support is not only affected by the Ni_n–support interaction, but is also affected by the Ni_n cluster and surface deformations, moreover, the Ni_n cluster deformation cannot be neglected except for the Ni_4 cluster due to the high stability of the tetrahedron. The results we obtained in the study of Ni_n clusters are different from the results obtained in previous studies of Cu_n clusters,[51] which show that the deformation of $Cu_n(n = 1-4)$ clusters is negligible.

3.2.2   Dehydrated γ-Al_2O_3(110) surface. Detailed information on the adsorption of $Ni_n(n = 1-7)$ clusters on the dehydrated γ-Al_2O_3(110) surface is given in the ESI† and the corresponding key geometrical parameters of the most stable adsorption configurations are also listed in Table 2.

We found that the Ni–Ni bond length of adsorbed $Ni_n(n = 2-7)$ clusters is longer than that of the isolated clusters, and increases with an increase of Ni_n cluster size, as a result, the Ni–Ni bond length gradually approaches the value in the bulk structure (2.492 Å). For adsorbed $Ni_n(n = 2-4)$ clusters, the corresponding cluster deformation is very weak, and makes a negligible

Table 2 The adsorption energy, E_{ads}, Ni_n metal–support interaction energy, E_{MSI}, Ni_n cluster deformation energy, E_{def,Ni_n}, surface deformation energy, $E_{def,surface}$, and the average Ni–Ni bond distance $\bar{d}$(Ni–Ni) for the most stable adsorption configuration of $Ni_n (n = 1–7)$ clusters on three different γ-Al$_2$O$_3$ surfaces

n	E_{ads}/kJ mol^{-1}	E_{MSI}/kJ mol^{-1}	E_{def,Ni_n}/kJ mol^{-1}	$E_{def,surface}$/kJ mol^{-1}	$\bar{d}$(Ni–Ni)/Å
Dehydrated γ-Al$_2$O$_3$(100) surface					
1	−352.2	−476.2	—	124.0	—
2	−480.3	−750.4	50.9	219.2	2.603
3	−374.4	−569.1	41.6	153.1	2.501
4	−442.8	−567.3	3.9	120.6	2.377
5	−431.7	−600.1	40.2	128.2	2.362
6	−464.7	−706.0	36.4	204.9	2.434
7	−493.5	−658.0	42.6	121.9	2.427
Dehydrated γ-Al$_2$O$_3$(110) surface					
1	−269.9	−359.4	—	89.5	—
2	−408.8	−540.7	3.5	128.4	2.251
3	−483.6	−623.2	6.7	132.9	2.366
4	−578.9	−730.3	6.0	145.4	2.377
5	−571.2	−859.6	95.4	193.0	2.434
6	−602.9	−870.1	64.5	202.7	2.477
7	−563.1	−813.8	52.6	198.1	2.463
Hydrated γ-Al$_2$O$_3$(110) surface					
1	−277.6	−331.6	—	54.0	—
2	−349.9	−449.6	0.8	98.9	2.204
3	−470.3	−572.0	1.4	100.3	2.281
4	−524.2	−625.5	9.3	92.0	2.387
5	−504.1	−656.9	29.4	123.4	2.426
6	−524.0	−702.0	41.8	136.2	2.452
7	−500.5	−652.0	40.1	111.4	2.404

contribution to the adsorption energy. However, beginning with Ni$_5$ clusters, the cluster deformation increases sharply, and cannot be neglected. On the other hand, for $Ni_n (n \geq 5)$ clusters, the surface deformation changes slightly. The results presented above indicate that when the number of Ni atoms in $Ni_n (n = 1–7)$ clusters is 5 or more, the adsorption can lead to a strong Ni_n cluster deformation, however, the adsorption cannot lead to a large change of surface deformation.

3.2.3 Hydrated γ-Al$_2$O$_3$(110) surface. Similar to the dehydrated γ-Al$_2$O$_3$(110) surface, the corresponding key geometrical parameters of the most stable adsorption configurations are also listed in Table 2. We found that for $Ni_n (n = 2–4)$ clusters, the cluster deformation has little effect on the adsorption energy, however, for $Ni_n (n \geq 5)$ clusters, the effect of cluster deformation cannot be neglected. Meanwhile, the Ni_n–support interaction contributes considerably to the adsorption ability. For $Ni_n (n = 1–7)$ clusters, the adsorption energy and the Ni_n–support interaction energy have the same varying tendency with an increase of $Ni_n (n = 1–7)$ cluster size, which is consistent with those on the dehydrated (110) surface.

On the other hand, compared to the dehydrated (110) surface, both the adsorption energy of $Ni_n (n = 2–7)$ clusters and the Ni_n–support interaction energy increase due to the presence of surface hydroxyls, whereas, for single Ni atoms, the adsorption energy decreases because of the weaker surface deformation. For $Ni_n (n = 1–7)$ clusters, the surface deformation of the

hydrated (110) surface is weaker than that of the dehydrated (110) surface, namely, the presence of surface hydroxyls can make the (110) surface more stable. Similarly, the adsorption of $Rh_n (n = 1–5)$ on both dehydrated and hydrated γ-Al$_2$O$_3$(100) surfaces also shows that the presence of surface hydroxyls is favorable for the stability of the γ-Al$_2$O$_3$ surface.[49] Meanwhile, for $Ni_n (n \geq 5)$ clusters, due to the presence of surface hydroxyls, cluster deformation on the hydrated γ-Al$_2$O$_3$(110) surface is weaker than that on the dehydrated γ-Al$_2$O$_3$(110) surface, which means that the surface hydroxyls can reduce the effect of the support on the adsorbed cluster.

3.2.4 Brief summary about stability. On the basis of the above studies of the adsorption of $Ni_n (n = 1–7)$ clusters on three different γ-Al$_2$O$_3$ surfaces, we firstly deduced that there is a strong correlation between the adsorption energy of Ni_n clusters, cluster deformation energy, surface deformation energy, and Ni_n–support interaction energy, suggesting that the adsorption stability of $Ni_n (n = 1–7)$ clusters on the γ-Al$_2$O$_3$ surface is not only affected by the Ni_n–support interaction, but is also affected by the cluster and surface deformations, in which the deformation of the $Ni_n (n = 2–7)$ clusters on the dehydrated γ-Al$_2$O$_3$(100) surface cannot be neglected except for Ni$_4$ clusters due to the high stability of the tetrahedron, however, for the γ-Al$_2$O$_3$(110) surface, the deformation of the $Ni_n (n = 2–4)$ clusters is negligible. Meanwhile, due to the stronger Ni_n–support interaction, $Ni_n (n = 3–7)$ clusters are much more stably adsorbed on the γ-Al$_2$O$_3$(110) surface than the corresponding cluster on the γ-Al$_2$O$_3$(100) surface, however, for single Ni atoms and Ni$_2$ clusters, the reverse becomes true.

Secondly, for the γ-Al$_2$O$_3$(110) surface, due to the weaker surface deformation, the adsorption stability of single Ni atoms on the hydrated surface is stronger than that on the dehydrated surface. Whereas, for $Ni_n (n = 2–7)$ clusters, both the adsorption energy and the Ni_n–support interaction energy for the hydrated surface are higher than those for the dehydrated surface, indicating that surface hydroxyls have a negative effect on the adsorption stability of $Ni_n (n = 2–7)$ clusters, and reduce the interaction between the Ni_n clusters and the γ-Al$_2$O$_3$ surface, which is in accordance with the previous studies.[32,49] Meanwhile, the surface deformation of the hydrated surface is weaker than that of the dehydrated surface, namely, the presence of surface hydroxyls can improve the stability of the (110) surface. Moreover, for $Ni_n (n \geq 5)$ clusters, the cluster deformation is much larger than that of the $Ni_n (n = 2–4)$ clusters, and the cluster deformation of $Ni_n (n \geq 5)$ clusters on the hydrated surface is weaker than that on the dehydrated surface, which means that the surface hydroxyls can reduce the effect of the support on the adsorbed cluster.

On the other hand, to probe into the effect of the support and surface hydroxyls on the stability of $Ni_n (n = 2–7)$ clusters, the average binding energy of supported $Ni_n (n = 2–7)$ clusters on three different γ-Al$_2$O$_3$ surfaces, $E_{bind}(Ni_n/\gamma$-Al$_2$O$_3)$, was calculated, as listed in Table 3.

$E_{bind}(Ni_n/\gamma$-Al$_2$O$_3)$ is given by the following equation:[51,53]

$$E_{bind}(Ni_n/\gamma\text{-Al}_2O_3) = [E(Ni_n/\gamma\text{-Al}_2O_3) - n \times E(Ni) - E(\gamma\text{-Al}_2O_3)]/n$$

herein, $n = 2–7$. $E_{bind}(Ni_n/\gamma\text{-}Al_2O_3)$ reflects the stability of Ni_n clusters supported on the $\gamma\text{-}Al_2O_3$ support surface, the small value of $E_{bind}(Ni_n/\gamma\text{-}Al_2O_3)$ denotes that the Ni_n clusters supported on the $\gamma\text{-}Al_2O_3$ surface are more stable.

Our results show that the average binding energy of $Ni_n(n = 2–7)$ clusters in the supported state is higher than that in the corresponding isolated state, which means that the support can stabilize the $Ni_n(n = 2–7)$ clusters well. Meanwhile, the stability of the supported $Ni_n(n = 3–7)$ clusters on the $\gamma\text{-}Al_2O_3(110)$ surface is better than that on the $\gamma\text{-}Al_2O_3(100)$ surface, however, for Ni_2 clusters, the reverse becomes true. For the $\gamma\text{-}Al_2O_3(110)$ surface, the stability of the supported $Ni_n(n = 2–7)$ clusters on the dehydrated surface is better than that on the hydrated surface, namely, surface hydroxyls reduce the stability of the supported Ni_n clusters.

3.3 Nucleation of Ni_n cluster on the different $\gamma\text{-}Al_2O_3$ surfaces

Based on the above stable adsorption configurations of $Ni_n(n = 1–7)$ clusters on the different $\gamma\text{-}Al_2O_3$ surfaces, the nucleation of Ni_n clusters on the different $\gamma\text{-}Al_2O_3$ surfaces has been further discussed. The nucleation is defined as the chemical reaction of $Ni_{n−1}/\gamma\text{-}Al_2O_3 + Ni_1/\gamma\text{-}Al_2O_3 = Ni_n/\gamma\text{-}Al_2O_3$, and the corresponding nucleation energy is calculated as follows:[51]

$$E_{nuc} = E(Ni_n/\gamma\text{-}Al_2O_3) + E(\gamma\text{-}Al_2O_3) - E(Ni_{n-1}/\gamma\text{-}Al_2O_3) - E(Ni_1/\gamma\text{-}Al_2O_3)$$

where $E(Ni_{n−1}/\gamma\text{-}Al_2O_3)$ is the total energy of the $\gamma\text{-}Al_2O_3$ slab together with the $Ni_{n−1}$ clusters, and $E(Ni_1/\gamma\text{-}Al_2O_3)$ is the total energy of the $\gamma\text{-}Al_2O_3$ slab together with a single Ni atom. The nucleation energy indicates the energy gained (or lost) when an adsorbed atom is combined with a $Ni_{n−1}$ cluster to form a Ni_n cluster, and the negative value denotes that the nucleation of the Ni_n cluster is exothermic, and is thermodynamically favorable, whereas, the positive value denotes that the nucleation of the Ni_n cluster is endothermic, and thermodynamically unfavorable.

Table 4 lists the calculated nucleation energies on different surfaces together with the corresponding isolated Ni_n cluster. We can see that on the dehydrated (100) surface, the nucleation

of $Ni_n(n = 2–7)$ clusters is not thermodynamically favored, namely, the dehydrated (100) surface is unfavorable for the nucleation of Ni clusters. On the dehydrated (110) surface, the nucleation of all the Ni clusters is exothermic, whereas, on the hydrated (110) surface, the nucleation of Ni_2 clusters is thermodynamically unfavorable; however, for the Ni_n clusters with 3 or more Ni atoms, the nucleation becomes favorable, which means that the critical cluster size for Ni cluster nucleation on the hydrated (110) surface is 3. More importantly, the exothermicity of supported $Ni_n(n = 2–7)$ clusters on different $\gamma\text{-}Al_2O_3$ surfaces is lower than that of isolated Ni_n clusters, which means that the support can reduce the nucleation ability of $Ni_n(n = 2–7)$ clusters, therefore, the support can inhibit the aggregation of clusters, and favors the formation of highly dispersed Ni particles to prevent their sintering into supranano ones. This result is in agreement with previous studies on the nucleation of Pd,[48] Rh,[49] Cu[51] and Pt[80] on $\gamma\text{-}Al_2O_3$ surfaces.

On the other hand, for the nucleation energy of $Ni_n(n = 2–7)$ clusters, the $\gamma\text{-}Al_2O_3(110)$ surface is weaker than the $\gamma\text{-}Al_2O_3(100)$ surface, namely, the nucleation of $Ni_n(n = 2–7)$ clusters is preferred on the $\gamma\text{-}Al_2O_3(110)$ surface compared to the $\gamma\text{-}Al_2O_3(100)$ surface. For the $\gamma\text{-}Al_2O_3(110)$ surface, the nucleation energy of $Ni_n(n = 2–7)$ clusters on the dehydrated surface is lower than that on the hydrated surface except for Ni_3 clusters, suggesting that the nucleation of $Ni_n(n = 2–7)$ clusters is preferred on the dehydrated (110) surface, namely, the presence of surface hydroxyls reduces the nucleation ability of $Ni_n(n = 2–7)$ clusters.

Further, although the $Ni/\gamma\text{-}Al_2O_3$ catalyst has been widely studied both experimentally and theoretically,[27,81–89] these studies have all focussed on the effect of Ni particle size on the target reaction or products, for example, the studies by Chen et al.[83] have reported CH_4 decomposition over supported Ni catalysts with different Ni particle sizes, suggesting that the smaller sizes of Ni particles give lower carbon yield. Meanwhile, the support plays a key role in the particle size, metal–support interactions, as well as Ni particle crystallographic orientations. Thus, the support has a significant effect on the structure of the target product nanofibers and carbon yield. The effect of various supports has been investigated.[86–89] Up to now, to our knowledge, little attention has been paid to the effect of $\gamma\text{-}Al_2O_3$ surface hydroxylation on the stability and nucleation of Ni in a for $Ni/\gamma\text{-}Al_2O_3$ catalyst, meanwhile, the effect of the support

Table 3 The binding energy of $Ni_n(n = 2–7)$ clusters supported on the different $\gamma\text{-}Al_2O_3$ surfaces per metallic atoms for the most stable adsorption configuration, $E_{bind}(Ni_n/\gamma\text{-}Al_2O_3)$, and the binding energy of isolated $Ni_n(n = 2–7)$ clusters, $E_{bind}(Ni_n)$

	$E_{bind}(Ni_n)$/kJ per mol per atom	$E_{bind}(Ni_n/\gamma\text{-}Al_2O_3)$/kJ per mol per atom		
n	Isolated	Dehydrated (100)	Dehydrated (110)	Hydrated (110)
2	−98.6	−338.8	−303.0	−273.5
3	−144.5	−269.3	−305.7	−301.2
4	−171.1	−281.8	−315.8	−302.1
5	−198.9	−285.2	−313.1	−297.1
6	−211.9	−289.4	−312.4	−295.6
7	−227.7	−298.2	−308.1	−299.2

Table 4 The nucleation energy E_{nuc} of $Ni_n(n = 2–7)$ clusters supported on three different $\gamma\text{-}Al_2O_3$ surfaces, and the isolated $Ni_n(n = 2–7)$ clusters

	E_{nuc}/kJ mol^{-1}			
n	Dehydrated (100)	Dehydrated (110)	Hydrated (110)	Isolated
2	26.8	−66.2	8.1	−197.2
3	221.8	−41.1	−79.1	−236.3
4	32.8	−76.3	−27.2	−250.9
5	53.4	−32.3	−12.2	−309.9
6	41.9	−39.1	−10.3	−277.2
7	1.0	−12.6	−21.2	−322.4

surface properties on Ni particle sizes, Ni-support interactions, and Ni morphology has not been systematically well-studied. Recently, only Briquet et al.[90–92] have investigated the adsorption of the single Ni atom on the clean and hydrated (0001) surface of α-Al$_2$O$_3$, as well as the adsorption of Ni$_6$ cluster on the clean (0001) surface, suggesting that the adsorption on hydrated surfaces is different from that on the clean surface, strong stabilization of the single Ni atom by the hydroxyl group was observed, which agrees with our calculated result. The studies by Li et al.[93] have investigated the adsorption of the tetrahedrally configured Ni$_4$ cluster on a γ-Al$_2$O$_3$(100) surface, the optimized stable configuration was different, the corresponding adsorption energy in our study was much higher than that obtained by Li et al., thus, the optimized Ni$_4$/γ-Al$_2$O$_3$(100) configuration in our study is thought to be the most stable.

On the basis of the above reported results, we obtained little information on the systematic investigation of the effect of γ-Al$_2$O$_3$ surface hydroxylation on the stability and nucleation of different sized Ni$_n$($n = 2$–7) cluster in Ni/γ-Al$_2$O$_3$ catalysts, to carry out a comparison between our results and previously reported results. However, a large number of studies have focussed on the effect of γ-Al$_2$O$_3$ surface hydroxylation on the stability and nucleation of Pd,[48] Rh,[49] Cu[51] and Pt[80] on the γ-Al$_2$O$_3$ surface, thus, a comparison of the stability and nucleation of Ni with that of other metals Pd, Rh, Cu and Pt was carried out and is presented in the following section.

3.4 Comparison of the stability and nucleation of Ni with that of other metals Pt, Rh, Pd and Cu

On the basis of the nucleation of Ni, in this section, we made a simple comparison with previous studies on the nucleation of other metals Pt, Rh, Pd and Cu. Our results show that the most stable configurations of Pd,[48] Rh,[49] Cu,[51] Pt[80] and Ni on the γ-Al$_2$O$_3$ surface are quite different, only on the γ-Al$_2$O$_3$(100) surface does the adsorption of single Pt atoms have a similar stable configuration to that of single Ni atoms, indicating that when different metals with the same size are adsorbed on the same γ-Al$_2$O$_3$ surface, they correspond to different adsorption sites and the most stable configurations. Meanwhile, the studies by Briquet et al.[90–92] have shown that the interaction of single Ni atoms on the α-Al$_2$O$_3$(0001) surface results in less exothermic values (close to 170 kJ mol^{-1}) compared to those on different γ-Al$_2$O$_3$ surfaces, this may be explained by the higher coordination of Al and O surface atoms of the α-Al$_2$O$_3$(0001) surface compared to the γ-Al$_2$O$_3$ surface, thus, the γ-Al$_2$O$_3$ surface has a higher intrinsic surface reactivity than the α-Al$_2$O$_3$ surface. Further, the nucleation of Pd,[48] Rh,[49] Cu[51] and Ni also differs, firstly, on the dehydrated (100) surface, the nucleation energy of Pd$_n$($n = 1$–5) clusters is positive until $n = 4$, namely, the critical cluster size of Pd is 4; for Rh$_n$($n = 1$–5) and Cu$_n$($n = 1$–4) clusters, it is 3; however, for the Ni$_n$($n = 1$–7) cluster in this study, the nucleation energy was always positive, which means that the critical cluster size for Ni is greater than 7. Secondly, on the hydrated (110) surface, the critical cluster size of Pd is 3; for Rh and Cu, it is 2; while for Ni in this study, it was 3. Thirdly, on the dehydrated (110) surface, the critical cluster size of Cu and Ni is 2.

On the other hand, the nucleation of Rh$_n$($n = 1$–5) clusters is preferred on the hydrated γ-Al$_2$O$_3$ surface relative to that on the dehydrated γ-Al$_2$O$_3$ surface. For Pd$_n$($n = 1$–5) clusters, nucleation at very low metal coverage on an hydrated surface is more favorable than that on a dehydrated surface, whereas, at a higher metal coverage, the reverse becomes true. For Cu and Ni clusters, compared to the γ-Al$_2$O$_3$(100) surface, the γ-Al$_2$O$_3$(110) surface is more favorable for the nucleation of Cu and Ni clusters, in which surface hydroxyls reduce the nucleation ability of Cu and Ni clusters. In addition, Mager-Maury et al.[80] carried out studies on the adsorption of Pt$_n$ clusters ($1 \leq n \leq 5$ and $n = 13$) on four γ-Al$_2$O$_3$ surfaces to investigate their stability as a function of particle's size, suggesting that the migration of H and Cl on γ-Al$_2$O$_3$ surfaces induces a stronger interaction for the Pt$_3$ cluster, which is thus proposed to be at the origin of the formation of highly dispersed platinum particles.

4. Conclusions

The effect of γ-Al$_2$O$_3$ surface hydroxylation on the stability and nucleation of Ni$_n$($n = 1$–7) clusters over dehydrated γ-Al$_2$O$_3$(100), dehydrated γ-Al$_2$O$_3$(110) and hydrated γ-Al$_2$O$_3$(110) surfaces has been systematically investigated by the DFT method. The results show that the Ni$_n$–support interaction mainly contributes to the stability of Ni$_n$($n = 1$–7) clusters on the three different γ-Al$_2$O$_3$ surfaces, Ni$_n$($n = 3$–7) clusters on the γ-Al$_2$O$_3$(110) surface are much more stable than the corresponding clusters on the γ-Al$_2$O$_3$(100) surface, whereas, for single Ni atoms and Ni$_2$ clusters, the reverse becomes true. For the γ-Al$_2$O$_3$(110) surface, surface hydroxyls do not favor the adsorption stability of Ni$_n$($n = 2$–7) clusters, and lower the interaction between the Ni$_n$ clusters and the γ-Al$_2$O$_3$ surface, however, surface hydroxyls increase the surface stability of γ-Al$_2$O$_3$(110).

The critical cluster size for the nucleation of Ni$_n$($n = 2$–7) clusters on the hydrated γ-Al$_2$O$_3$(110) surface is 3, while on the dehydrated (100) surface, the critical cluster size should be greater than 7. Meanwhile, from the viewpoint of thermodynamics, the nucleation of Ni$_n$ clusters on different γ-Al$_2$O$_3$ surfaces show different trends with an increase of the Ni$_n$($n = 2$–7) cluster size. For the exothermicity of the nucleation, the supported Ni$_n$($n = 2$–7) clusters are smaller than the isolated Ni$_n$($n = 2$–7) clusters, suggesting that the support can reduce the nucleation ability of Ni$_n$($n = 2$–7) clusters. Further, for the nucleation of Ni$_n$($n = 2$–7) clusters on the support, the γ-Al$_2$O$_3$(110) surface is more favorable than the γ-Al$_2$O$_3$(100) surface. Finally, for the γ-Al$_2$O$_3$(110) surface, the nucleation of Ni$_n$($n = 2$–7) clusters preferably occurs on a dehydrated surface, indicating that surface hydroxyls can lower the nucleation ability of Ni$_n$ clusters. Therefore, the γ-Al$_2$O$_3$ support and its surface hydroxyls can inhibit the aggregation of clusters, and favor the formation of highly dispersed Ni particles preventing their sintering into supranano ones.

Acknowledgements

their helpful suggestions on the quality improvement of our present paper.

References

1 V. E. Henrich and P. A. Cox, *The Surface Science of Metal Oxides*, Cambridge University Press, Cambridge, U.K, 1994.

2 G. Ertl, H. Knözinger and J. Weitkamp, *Handbook of Heterogeneous Catalysis*, Wiley Company, Weinheim, 1997.

3 D. Nazimek, A. Machocki and T. Borowiecki, The Influence of Nickel Dispersion in Ni/Al$_2$O$_3$ Catalysts on Their Properties in the Reaction with Hydrogen, Hydrocarbons and Steam, *Adsorpt. Sci. Technol.*, 1998, **16**, 747–757.

4 J. P. Jacobs, L. P. Lindfors, J. G. H. Reintjes, O. Jylhä and H. H. Brongersma, The Growth Mechanism of Nickel in the Preparation of Ni/Al$_2$O$_3$ Catalysts Studied by LEIS, XPS and Catalytic Activity, *Catal. Lett.*, 1994, **25**, 315–324.

5 T. J. Šarapatka, XPS-XAES Study of Charge Transfers at Ni/Al$_2$O$_3$/Al Systems, *Chem. Phys. Lett.*, 1993, **212**, 37–42.

6 F. Loviat, I. Czekaj, J. Wambach and A. Wokaun, Nickel Deposition on γ-Al$_2$O$_3$ Model Catalysts: An Experimental and Theoretical Investigation, *Surf. Sci.*, 2009, **603**, 2210–2217.

7 A. N. Fatsikostas and X. E. Verykios, Reaction Network of Steam Reforming of Ethanol over Ni-based Catalysts, *J. Catal.*, 2004, **225**, 439–452.

8 J. Zhou, Y. C. Kang and D. A. Chen, Controlling Island Size Distributions: A Comparison of Nickel and Copper Growth on TiO$_2$(110), *Surf. Sci.*, 2003, **537**, L429–L434.

9 Y. W. Zhang, Z. H. Wang, J. H. Zhou, J. Z. Liu and K. Cen, Catalytic Decomposition of Hydrogen Iodide over Pre-treated Ni/CeO$_2$ Catalysts for Hydrogen Production in the Sulfur-iodine Cycle, *Int. J. Hydrogen Energy*, 2009, **34**, 8792–8798.

10 M. A. Keane, G. Jacobs and P. M. Patterson, Ni/SiO$_2$ Promoted Growth of Carbon Nanofibers from Chlorobenzene: Characterization of the Active Metal Sites, *J. Colloid Interface Sci.*, 2006, **302**, 576–588.

11 A. Venugopal, S. N. Kumar, J. Ashok, H. D. Prasad, V. D. Kumari, K. B. S. Prasad and M. Subrahmanyam, Hydrogen Production by Catalytic Decomposition of Methane over Ni/SiO$_2$, *Int. J. Hydrogen Energy*, 2007, **32**, 1782–1788.

12 P. Euzen, P. Raybaud, X. Krokidis, H. Toulhoat, J. L. Le Loarer, J. P. Jolivet and C. Froidefond, in *Handbook of Porous Solids*, ed. F. Schüth, K. S. W. Sing and J. Weitkamp, Wiley–VCH, Weinheim, 2002, pp. 1591–1677.

13 A. Dey, Y. I. Jiang, P. O. de Montellano, K. O. Hodgson, B. Hedman and E. I. Solomon, S K-edge XAS and DFT Calculations on Cytochrome P450: Covalent and Ionic Contributions to the Cysteine-Fe Bond and Their Contribution to Reactivity, *J. Am. Chem. Soc.*, 2009, **131**, 7869–7878.

14 S. P. de Visser and L. S. Tan, Is the Bound Substrate in Nitric Oxide Synthase Protonated or Neutral and What Is the Active Oxidant that Performs Substrate Hydroxylation?, *J. Am. Chem. Soc.*, 2008, **130**, 12961–12974.

15 M. Digne, P. Raybaud, P. Sautet, D. Guillaume and H. Toulhoat, Atomic Scale Insights on Chlorinated γ-Alumina Surfaces, *J. Am. Chem. Soc.*, 2008, **130**, 11030–11039.

16 X. D. Xu and P. Servati, Facet-Dependent Electronic Properties of Hexagonal Silicon Nanowires under Progressive Hydroxylation and Surface Reconstruction, *Nano Lett.*, 2009, **9**, 1999–2004.

17 Z. L. Hong, L. F. Cheng, L. T. Zhang and Y. G. Wang, Water Vapor Corrosion Behavior of Scandium Silicates at 1400 °C, *J. Am. Ceram. Soc.*, 2009, **92**, 193–196.

18 A. Arranz, C. Palacio, D. Garcia-Fresnadillo, G. Orellana, A. Navarro and E. Muñoz, Influence of Surface Hydroxylation on 3-Aminopropyltriethoxysilane Growth Mode during Chemical Functionalization of GaN Surfaces: An Angle-Resolved X-ray Photoelectron Spectroscopy Study, *Langmuir*, 2008, **24**, 8667–8671.

19 J. A. Rodriguez, J. Evans, J. Graciani, J.-B. Park, P. Liu, J. Hrbek and J. F. Sanz, High Water–Gas Shift Activity in TiO$_2$(110) Supported Cu and Au Nanoparticles: Role of the Oxide and Metal Particle Size, *J. Phys. Chem. C*, 2009, **113**, 7364–7370.

20 Z. P. Qu, W. X. Huang, S. T. Zhou, H. Zheng, X. M. Liu, M. J. Cheng and X. H. Bao, Enhancement of the Catalytic Performance of Supported-Metal Catalysts by Pretreatment of the Support, *J. Catal.*, 2005, **234**, 33–36.

21 M. Daturi and L. G. Appel, Infrared Spectroscopic Studies of Surface Properties of Mo/SnO$_2$ Catalyst, *J. Catal.*, 2002, **209**, 427–432.

22 D. Lomot and Z. Karpinski, The effect of Pd/Al$_2$O$_3$ Pretreatment on Catalytic Activity in Cyclopentane/Deuterium Exchange, *Catal. Lett.*, 2000, **69**, 133–138.

23 C. J. Bertole, C. A. Mims and G. Kiss, The Effect of Water on the Cobalt-Catalyzed Fischer–Tropsch Synthesis, *J. Catal.*, 2002, **210**, 84–96.

24 F. G. Botes, The Effects of Water and CO$_2$ on the Reaction Kinetics in the Iron-Based Low-Temperature Fischer-Tropsch Synthesis: A Literature Review, *Catal. Rev. Sci. Eng.*, 2008, **50**, 471–491.

25 M. C. Valero, P. Raybaud and P. Sautet, Interplay between Molecular Adsorption and Metal–Support Interaction for Small Supported Metal Clusters: CO and C$_2$H$_4$ Adsorption on Pd$_4$/γ-Al$_2$O$_3$, *J. Catal.*, 2007, **247**, 339–355.

26 S. X. Yin, T. Swift and Q. F. Ge, Adsorption and Activation of CO$_2$ over the Cu-Co Catalyst Supported on Partially Hydroxylated γ-Al$_2$O$_3$, *Catal. Today*, 2011, **165**, 10–18.

27 Y. X. Pan, C. J. Liu and Q. F. Ge, Effect of Surface Hydroxyls on Selective CO$_2$ Hydrogenation Over Ni$_4$/γ-Al$_2$O$_3$: A Density Functional Theory Study, *J. Catal.*, 2010, **272**, 227–234.

28 Y. X. Pan, C. J. Liu, T. S. Wiltowski and Q. F. Ge, CO$_2$ Adsorption and Activation Over γ-Al$_2$O$_3$-Supported Transition Metal Dimers: A Density Functional Study, *Catal. Today*, 2009, **147**, 68–76.

29 Y. X. Pan, C. J. Liu and Q. F. Ge, Adsorption and Protonation of CO$_2$ on Partially Hydroxylated γ-Al$_2$O$_3$ Surfaces: A Density Functional Theory Study, *Langmuir*, 2008, **24**, 12410–12419.

30 M. C. Valero, P. Raybaud and P. Sautet, Influence of the Hydroxylation of γ-Al$_2$O$_3$ Surfaces on the Stability and

Diffusion of Single Pd Atoms: A DFT Study, *J. Phys. Chem. B*, 2006, **110**, 1759–1767.

31 R. G. Zhang, H. Y. Liu, B. J. Wang and L. X. Ling, Insights into the Effect of Surface Hydroxyls on CO_2 Hydrogenation Over Pd/γ-Al_2O_3 Catalyst: A Computational Study, *Appl. Catal., B*, 2012, **126**, 108–120.

32 R. G. Zhang, B. J. Wang, H. Y. Liu and L. X. Ling, Effect of Surface Hydroxyls on CO_2 Hydrogenation Over Cu/γ-Al_2O_3 Catalyst: A Theoretical Study, *J. Phys. Chem. C*, 2011, **115**, 19811–19818.

33 B. Hvolbæk, T. V. W. Janssens, B. S. Clausen, H. Falsig, C. H. Christensen and J. K. Nøskov, Catalytic Activity of Au Nanoparticles, *Nano Today*, 2007, **2**, 14–18.

34 F. Li and B. C. Gates, Size-Dependent Catalytic Activity of Zeolite-Supported Iridium Clusters, *J. Phys. Chem. C*, 2007, **111**, 262–267.

35 A. M. Argo, J. F. Odzak and B. C. Gates, Role of Cluster Size in Catalysis: Spectroscopic Investigation of γ-Al_2O_3-Supported Ir_4 and Ir_6 during Ethene Hydrogenation, *J. Am. Chem. Soc.*, 2003, **125**, 7107–7115.

36 M. Montano, K. Bratlie, M. Salmeron and G. A. Somorjai, Hydrogen and Deuterium Exchange on Pt(111) and Its Poisoning by Carbon Monoxide Studied by Surface Sensitive High-Pressure Techniques, *J. Am. Chem. Soc.*, 2006, **128**, 13229–13234.

37 N. S. Babu, N. Lingaiah, R. Gopinath, P. S. S. Reddy and P. S. S. Prasad, Characterization and Reactivity of Alumina-Supported Pd Catalysts for the Room-Temperature Hydrodechlorination of Chlorobenzene, *J. Phys. Chem. C*, 2007, **111**, 6447–6453.

38 R. Gopinath, N. S. Babu, J. V. Kumar, N. Lingaiah and P. S. S. Prasad, Influence of Pd Precursor and Method of Preparation on Hydrodechlorination Activity of Alumina Supported Palladium Catalysts, *Catal. Lett.*, 2007, **120**, 312–319.

39 B. C. Gates, Supported Metal Cluster Catalysts, *J. Mol. Catal. A: Chem.*, 2000, **163**, 55–65.

40 D. C. Meier and D. W. Goodman, The Influence of Metal Cluster Size on Adsorption Energies: CO Adsorbed on Au Clusters Supported on TiO_2, *J. Am. Chem. Soc.*, 2004, **126**, 1892–1899.

41 Z. X. Cheng, X. G. Zhao, J. L. Li and Q. M. Zhu, Role of Support in CO_2 Reforming of CH_4 over a Ni/γ-Al_2O_3 Catalyst, *Appl. Catal., A*, 2001, **205**, 31–36.

42 P. G. Savva, K. Goundani, J. Vakros, K. Bourikas, C. Fountzoula, D. Vattis, A. Lycourghiotis and C. Kordulis, Benzene Hydrogenation over Ni/Al_2O_3 Catalysts Prepared by Conventional and Sol–Gel Techniques, *Appl. Catal., B*, 2008, **79**, 199–207.

43 S. Yolcular and Ö. Olgun, Ni/Al_2O_3 Catalysts and Their Activity in Dehydrogenation of Methylcyclohexane for Hydrogen Production, *Catal. Today*, 2008, **138**, 198–202.

44 A. S. A. Al-Fatish, A. A. Ibrahim, A. H. Fakeeha, M. A. Soliman, M. R. H. Siddiqui and A. E. Abasaeed, Coke Formation During CO_2 Reforming of CH_4 over Alumina-Supported Nickel Catalysts, *Appl. Catal., A*, 2009, **364**, 150–155.

45 A. E. Aksoylu and Z. İlsenÖnsan, Hydrogenation of Carbon Oxides Using Coprecipitated and Impregnated Ni/Al_2O_3 Catalysts, *Appl. Catal., A*, 1997, **164**, 1–11.

46 A. R. Suzdorf, S. V. Morozov, N. N. Anshits, S. I. Tsignova and A. G. Anshits, Gas Phase Hydrodechlorination of Chlorinated Aromatic Compounds on Nickel Catalysts, *Catal. Lett.*, 1994, **29**, 49–55.

47 S. Hernández, L. Solarino, G. Orsello, N. Russo, D. Fino, G. Saracco and V. Specchia, Desulfurization Processes for Fuel Cells Systems, *Int. J. Hydrogen Energy*, 2008, **33**, 3209–3214.

48 M. C. Valero, P. Raybaud and P. Sautet, Nucleation of Pd_n($n = 1$–5) Clusters and Wetting of Pd Particles on γ-Al_2O_3 Surfaces: A Density Functional Theory Study, *Phys. Rev. B: Condens. Matter Mater. Phys.*, 2007, **75**.

49 X. R. Shi and D. S. Sholl, Nucleation of Rh_n($n = 1$–5) Clusters on γ-Al_2O_3 Surfaces: A Density Functional Theory Study, *J. Phys. Chem. C*, 2012, **116**, 10623–10631.

50 N. C. Hernández, J. Graciani, A. Márquez and J. F. Sanz, Cu, Ag and Au Atoms Deposited on the α-Al_2O_3(0001) Surface: A Comparative Density Functional Study, *Surf. Sci.*, 2005, **575**, 189–196.

51 J. R. Li, R. G. Zhang and B. J. Wang, Influence of the Hydroxylation of γ-Al_2O_3 Surfaces on the Stability and Growth of Cu for Cu/γ-Al_2O_3 Catalyst: A DFT Study, *Appl. Surf. Sci.*, 2013, **270**, 728–736.

52 S. Nigam and C. Majumder, Growth Pattern of Ag_n($n = 1$–8) Clusters on the α-Al_2O_3(0001) Surface: A First Principles Study, *Langmuir*, 2010, **26**, 18776–18787.

53 C. H. Hu, C. Chizallet, C. Mager-Maury, M. Corral-Valero, P. Sautet, H. Toulhoat and P. Raybaud, Modulation of Catalyst Particle Structure upon Support Hydroxylation: *Ab Initio* Insights into Pd_{13} and Pt_{13}/γ-Al_2O_3, *J. Catal.*, 2010, **274**, 99–110.

54 M. C. Valero, M. Digne, P. Sautet and P. Raybaud, DFT Study of the Interaction of a Single Palladium Atom with γ-AluminaSurfaces: the Role of Hydroxylation, *Oil Gas Sci. Technol.*, 2006, **61**, 535–545.

55 M. Digne, P. Sautet, P. Raybaud, P. Euzen and H. Toulhoat, Use of DFT to Achieve a Rational Understanding of Acid–Basic Properties of γ-Alumina Surfaces, *J. Catal.*, 2004, **226**, 54–68.

56 G. Paglia, C. E. Buckley, A. L. Rohl, B. A. Hunter, R. D. Hart, J. V. Hanna and L. T. Byrne, Tetragonal Structure Model for Boehmite-Derived γ-Alumina, *Phys. Rev. B: Condens. Matter*, 2003, **68**.

57 G. Paglia, C. E. Buckley, A. L. Rohl and L. T. Byrne, Towards the Determination of the Structure of γ-Alumina, *J. Australas. Ceram. Soc.*, 2002, **38**, 92–98.

58 E. Menendez-Proupin and G. Gutierrez, Electronic Properties of Bulk γ-Al_2O_3, *Phys. Rev. B: Condens. Matter Mater. Phys.*, 2005, **72**.

59 G. Paglia, E. S. Bozǐn and S. J. L. Billinge, Fine-Scale Nanostructure in γ-Al_2O_3, *Chem. Mater.*, 2006, **18**, 3242–3248.

60 G. Paglia, C. E. Buckley and A. L. Rohl, Comment on "Examination of Spinel and Nonspinel Structural Models

for γ-Al$_2$O$_3$ by DFT and Rietveld Refinement Simulations", *J. Phys. Chem. B*, 2006, **110**, 20721–20723.

61 M. Digne, P. Raybaud, P. Sautet, B. Rebours and H. Toulhoat, Comment on "Examination of Spinel and Nonspinel Structural Models for γ-Al$_2$O$_3$ by DFT and Rietveld Refinement Simulations", *J. Phys. Chem. B*, 2006, **110**, 20719–20726.

62 X. Krokidis, P. Raybaud, A. E. Gobichon, B. Rebours, P. Euzen and H. Toulhoat, Theoretical Study of the Dehydration Process of Boehmite to γ-Alumina, *J. Phys. Chem. B*, 2001, **105**, 5121–5130.

63 M. Digne, P. Sautet, P. Raybaud, P. Euzen and H. Toulhoat, Hydroxyl Groups on γ-Alumina Surfaces: A DFT Study, *J. Catal.*, 2002, **211**, 1–5.

64 C. Wolverton and K. C. Hass, Phase Stability and Structure of Spinel-Based Transition Aluminas, *Phys. Rev. B: Condens. Matter*, 2000, **63**.

65 G. Paglia, A. L. Rohl, C. E. Buckley and J. D. Gale, Determination of the Structure of γ-Alumina from Interatomic Potential and First-Principles Calculations: The Requirement of Significant Numbers of Nonspinel Positions to Achieve an Accurate Structural Model, *Phys. Rev. B: Condens. Matter Mater. Phys.*, 2005, **71**.

66 J. P. Beaufils and Y. Barbaux, Détermination, Par Diffraction Différentielle de Neutrons, des Faces Cristallines Exposées par des Supports de Catalyseurs en Poudre, *J. Chim. Phys. Rev. Gen. Colloides*, 1981, **78**, 347–352.

67 P. Nortier and P. Fourre, Mohammed Saad, A. B.; Saur, O.; Lavalley, J. C. Effects of Crystallinity and Morphology on the Surface Properties of Alumina, *Appl. Catal.*, 1990, **61**, 141–160.

68 J. Libuda, M. Frank, A. Sandell, S. Andersson, P. A. Bruhwiler, M. Bäumer, N. Martensson and H. J. Freund, Interaction of Rhodium with Hydroxylated Alumina Model Substrates, *Surf. Sci.*, 1997, **384**, 106–119.

69 B. Delley, An All-Electron Numerical Method for Solving the Local Density Functional for Polyatomic Molecules, *J. Chem. Phys.*, 1990, **92**, 508–517.

70 B. Delley, From Molecules to Solids with the DMol^3 Approach, *J. Chem. Phys.*, 2000, **113**, 7756–7764.

71 J. P. Perdew, K. Burke and M. Ernzerhof, Generalized Gradient Approximation Made Simple, *Phys. Rev. Lett.*, 1996, **77**, 3865–3868.

72 P. Hohenberg and W. Kohn, Inhomogeneous Electron Gas, *Phys. Rev.*, 1964, **136**, B864–B871.

73 M. Dolg, U. Wedig, H. Stoll and H. Preuss, Energy-Adjusted *Ab Initio* Pseudopotentials for the First Row Transition Elements, *J. Chem. Phys.*, 1987, **86**, 866–872.

74 A. Bergner, M. Dolg, W. Küchle, H. Stoll and H. Preuss, *Ab Initio* Energy-Adjusted Pseudopotentials for Elements of Groups 13–17, *Mol. Phys.*, 1993, **80**, 1431–1441.

75 F. A. Reuse and S. N. Khanna, Geometry, Electronic Structure, and Magnetism of Small Ni$_n$(n = 2–6, 8, 13) Clusters, *Chem. Phys. Lett.*, 1995, **234**, 77–81.

76 M. D. Morse, G. P. Hansen, P. R. R. Langridge-Smith, L. S. Zheng, M. E. Gensic, D. L. Michalopoulos and R. E. Smalley, Spectroscopic Studies of the Jet-cooled Nickel Dimer, *J. Chem. Phys.*, 1984, **80**, 5400–5405.

77 J. Ho, M. L. Polak, K. M. Ervin and W. C. Lineberger, Photoelectron Spectroscopy of Nickel Group Dimmers: Ni$_2^-$, Pd$_2^-$, and Pt$_2^-$, *J. Chem. Phys.*, 1993, **99**, 8542–8551

78 S. Nigam and C. Majumder, Adsorption of Small Palladium Clusters on the α-Al$_2$O$_3$(0001) Surface: A First Principles Study, *J. Phys. Chem. C*, 2012, **116**, 2863–2871.

79 P. Liu, Understanding the Behavior of TiO$_2$(110)-Supported Pd$_7$ Cluster: A Density Functional Study, *J. Phys. Chem. C*, 2012, **116**, 25337–25343.

80 C. Mager-Maury, C. Chizallet, P. Sautet and P. Raybaud, Platinum Nanoclusters Stabilized on γ-Alumina by Chlorine Used as a Capping Surface Ligand: A Density Functional Theory Study, *ACS Catal.*, 2012, **2**, 1346–1357.

81 X. L. Zhu, D. G. Cheng and P. Kuai, Catalytic Decomposition of Methane over Ni/Al$_2$O$_3$ Catalysts: Effect of Plasma Treatment on Carbon Formation, *Energy Fuels*, 2008, **22**, 1480–1484.

82 L. B. Avdeeva, T. V. Reshetenko, Z. R. Ismagilov and V. A. Likholov, Iron-Containing Catalysts of Methane Decomposition: Accumulation of Filamentous Carbon, *Appl. Catal., A*, 2002, **228**, 53–63.

83 D. Chen, K. O. Christensen, E. Ochoa-Fernández, Z. X. Yu, B. Tøtdal, N. Latorre, A. Monzón and A. Holmen, Synthesis of Carbon Nanofibers: Effects of Ni Crystal Size During Methane Decomposition, *J. Catal.*, 2005, **229**, 82–96.

84 H. Dai, A. G. Rinzler, P. Nikolaev, A. Thess, D. T. Colbert and R. E. Smalley, Single-Wall Nanotubes Produced by Metal-Catalyzed Disproportionation of Carbon Monoxide, *Chem. Phys. Lett.*, 1996, **260**, 471–475.

85 C. L. Cheung, A. Kurtz, H. Park and C. M. Lieber, Diameter-Controlled Synthesis of Carbon Nanotubes, *J. Phys. Chem. B*, 2002, **106**, 2429–2433.

86 C. Park and M. A. Keane, Catalyst Support Effects in the Growth of Structured Carbon from the Decomposition of Ethylene over Nickel, *J. Catal.*, 2004, **221**, 386–399.

87 S. Takenaka, Y. Shigeta, E. Tanabe and K. Otuska, Methane Decomposition into Hydrogen and Carbon Nanofibers over Supported Pd–Ni Catalysts: Characterization of the Catalysts during the Reaction, *J. Phys. Chem. B*, 2004, **108**, 7656.

88 R. L. Van Wal, T. M. Ticich and V. E. Curtis, Substrate-Support Interactions in Metal-Catalyzed Carbon Nanofiber Growth, *Carbon*, 2001, **39**, 2277–2289.

89 X. N. Li, Y. Zhang and K. J. Smith, Metal–Support Interaction Effects on the Growth of Filamentous Carbon over Co/SiO$_2$ Catalysts, *Appl. Catal., A*, 2004, **264**, 81–91.

90 L. G. V. Briquet, C. R. A. Catlow and S. A. French, Comparison of the Adsorption of Ni, Pd, and Pt on the (0001) Surface of α-Alumina, *J. Phys. Chem. C*, 2008, **112**, 18948–18954.

91 L. G. V. Briquet, C. R. A. Catlow and S. A. French, Platinum Group Metal Adsorption on Clean and Hydroxylated Corundum Surfaces, *J. Phys. Chem. C*, 2009, **113**, 16747–16756.

92 L. G. V. Briquet, C. R. A. Catlow and S. A. French, Structure and Reactivity of Aluminum Oxide Supported Nickel Clusters, *J. Phys. Chem. C*, 2010, **114**, 22155–22158.

93 J. Li, E. Croiset and L. Ricardez-Sandoval, Effect of Metal–Support Interface During CH_4 and H_2 Dissociation on Ni/γ-Al_2O_3: A Density Functional Theory Study, *J. Phys. Chem. C*, 2013, **117**, 16907–16920.